THE JOURNAL OF PHYSICAL CHEMISTRY B

Article

pubs.acs.org/JPCB

Observation of a Continuous Random Network Structure in Ge_xSe_{100-x} Glasses: Results from High-Resolution ^{77}Se MATPASS/CPMG NMR Spectroscopy

Derrick C. Kaseman,[†] Ivan Hung,[‡] Zhehong Gan,[‡] and Sabyasachi Sen*,[†]

[†]Division of Materials Science, University of California, Davis, California 95616, United States

[‡]Center of Interdisciplinary Magnetic Resonance, National High Magnetic Field Laboratory, 1800 East Paul Dirac Drive, Tallahassee, Florida 32310, United States

ABSTRACT: The coordination environments of Se atoms in binary Ge_xSe_{100-x} glasses with $5 \leq x \leq 30$ are investigated using a novel, two-dimensional ^{77}Se nuclear magnetic resonance (NMR) spectroscopic technique. The high-resolution isotropic ^{77}Se NMR spectra allow for the identification of up to four distinct Se sites in these glasses. The chemical shift tensor parameters for these sites offer unique insights into their local site symmetries and nearest- and next-nearest-neighbor coordination environments. The structural results, when taken together, provide direct evidence in favor of the existence of a randomly connected network of $GeSe_4$ tetrahedra and Se−Se chain fragments in these glasses.

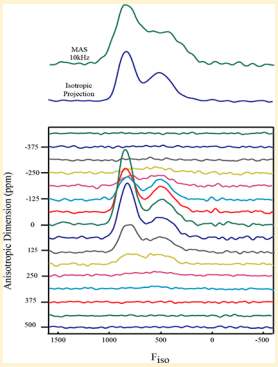

1. INTRODUCTION

The compositional flexibility of chalcogenide glasses in the form of continuous alloying allows for the tuning of a wide range of physical properties that has consequently enabled the technological applications of these materials in areas of photonics, telecommunication, and remote sensing.[1−3] Binary Ge_xSe_{100-x} glasses have served as model systems in understanding and developing structure−property relationships in complex chalcogenide glasses. The structures of Ge_xSe_{100-x} glasses have therefore been studied extensively in the literature using a wide variety of spectroscopic and diffraction techniques.[4−15] One of these techniques, ^{77}Se nuclear magnetic resonance (NMR) spectroscopy, has recently been established as a powerful tool for studying the short- and intermediate-range structural and topological characteristics of the Ge−Se network in Ge_xSe_{100-x} glasses.[8−10,13−15] ^{77}Se magic-angle spinning (MAS) NMR spectra of Ge_xSe_{100-x} glasses collected at a spinning rate of 15 kHz were interpreted by Sen and co-workers to be indicative of a network of randomly connected $GeSe_4$ tetrahedra and Se−Se chain fragments.[13,15] This interpretation was based on the claim that the simulation of the ^{77}Se MAS NMR spectra required a peak with an isotropic chemical shift near 570−590 ppm corresponding to Se−**Se**−Ge sites, in addition to the two main peaks centered at 830−850 and 370−390 ppm corresponding to Se−**Se**−Se and corner-shared (CS) Ge−**Se**−Ge sites, respectively. The presence of Se−**Se**−Ge sites indicates connectivity between the $GeSe_4$ tetrahedra and the Se−Se chain elements in the germanium selenide glass network. The compositional variation in the relative fractions of these three Se environments in Ge_xSe_{100-x} glasses, as expected from a randomly connected network of $GeSe_4$ tetrahedra and Se−Se chain fragments, is shown in Figure 1.[15] On the other hand, the ^{77}Se static NMR spectra of Ge_xSe_{100-x} glasses and supercooled liquids were simulated by Bureau and co-workers with only two peaks corresponding to the Se−**Se**−Se and Ge−**Se**−Ge sites.[8−10] The resulting "absence" of the Se−**Se**−Ge sites was consequently interpreted

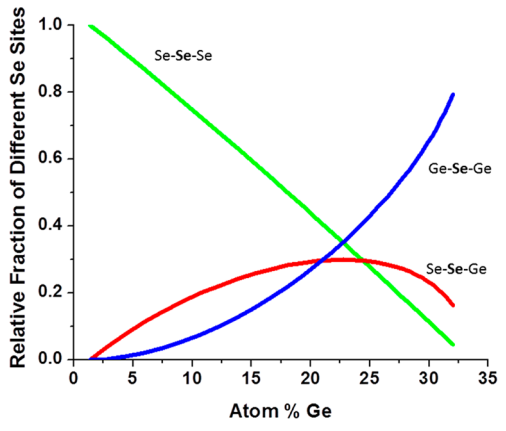

Figure 1. Compositional variation of the relative fractions of Se−**Se**−Se (green), Se−**Se**−Ge (red), and Ge−**Se**−Ge (blue) sites as predicted by the random network model.[15]

Received: November 15, 2012
Revised: December 26, 2012
Published: December 26, 2012

to be indicative of a spatial clustering of the tetrahedral and chain elements. It may be noted here that subsequently, density functional theory based ab initio calculations of ^{77}Se NMR chemical shifts of various Se sites in germanium selenides by Kibalchenko and co-workers indicated that indeed the isotropic ^{77}Se chemical shift δ_{iso} for the Se−**Se**−Ge sites would be located near 600 ppm.[16,17] These studies also indicated a similar δ_{iso} for the Ge−**Se**−Ge sites in edge-shared (ES) $GeSe_4$ tetrahedra in Ge_xSe_{100-x} glasses.

Therefore, the discrepancies between the structural scenarios for Ge_xSe_{100-x} glasses, as proposed by the ^{77}Se NMR spectroscopic studies in the literature, arise from somewhat subjective interpretation of the NMR spectra that suffered from lack of resolution, partially due to experimental limitations. Besides the structural disorder induced line broadening characteristic of amorphous materials, the ^{77}Se NMR line shapes of Ge_xSe_{100-x} glasses are also broadened by chemical shift anisotropy (CSA) for sites with noncubic site symmetry. This CSA-induced ^{77}Se NMR line broadening for the Ge_xSe_{100-x} glasses is in excess of ∼40−50 kHz depending on the magnetic field strength and cannot be fully averaged by MAS when the rotor spinning frequency is significantly smaller than the magnitude of the CSA. Although modern MAS NMR probes that use small rotors allow for sample spinning frequencies on the order ∼60 kHz, the correspondingly small sample size makes the acquisition of ^{77}Se NMR spectra with high signal-to-noise ratios practically impossible.

Two-dimensional (2D) NMR techniques can be employed to overcome the broadening from CSA interactions by manipulating the phases of the spinning sidebands to separate the isotropic chemical shift from the anisotropic chemical shift and allow their correlation to be determined in a single experiment. One such technique combines the idea of magic-angle turning and phase-adjusted sideband separation (MATPASS), allowing for isotropic/anisotropic chemical shift separation for disordered solids with line widths broadened by CSA far greater than the MAS frequency.[18,19] Carr−Purcell Meiboom−Gill (CPMG) echo train acquisition can be employed in combination with the 2D MATPASS technique to enhance the sensitivity for nuclides such as ^{77}Se.[18] In the present study, high-resolution ^{77}Se 2D MATPASS/CPMG NMR is used to identify and quantify the Se environments in binary Ge_xSe_{100-x} glasses ($5 \le x \le 30$), with high accuracy on the basis of their ^{77}Se isotropic chemical shifts and corresponding anisotropy. The results resolve the longstanding controversy in the literature regarding the nature of the intermediate-range order and connectivity between various Se environments in the network structure of these glasses.

2. EXPERIMENTAL SECTION

2.1. Synthesis. The Ge_xSe_{100-x} glasses with $5 \le x \le 30$ were synthesized in 5−10 g batches by melting mixtures of the constituent elements Ge and Se with ≥99.995% purity (metals basis) in evacuated (10^{-6} Torr) and flame-sealed fused silica ampules (8 mm i.d., 11 mm o.d.) at temperatures ranging between 1000 and 1200 K for up to 48 h in a rocking furnace. The ampules were subsequently quenched in water.

2.2. NMR Spectroscopy. All NMR measurements were carried out using a 19.6 T narrow bore magnet equipped with a Bruker DRX console at a resonance frequency of 158.8 MHz for ^{77}Se. A home-built 4 mm probe with a Samoson MAS stator was used. Crushed glass samples were packed into ZrO_2 rotors and spun at 10 kHz. For each 2D experiment, 16 hypercomplex t_1 points were acquired with 96 transients per point and 64 CPMG echoes per transient, in ∼51 h.[18] The details of the 2D MATPASS/CPMG pulse sequence can be found elsewhere.[18] Each transient was obtained using the MAT sequence of five π-pulses with interpulse delays that were incremented according to the timings detailed in ref 18. The MAT sequence was followed by CPMG pulses for multiple-echo acquisition. Hypercomplex data acquisition was employed by applying the method of States et al.[20] to the phases of the CPMG pulses and the receiver. The $\pi/2$- and π-pulse lengths were 2.0 and 4.0 μs, respectively, and a 60 s recycle delay was used. All spectra were externally referenced to a saturated H_2SeO_3 solution with a ^{77}Se isotropic chemical shift of δ_{iso} = 1282 ppm.

Because CSA increases linearly with the magnetic field, it can be argued that ^{77}Se NMR measurements at low magnetic field would result in smaller line widths and, therefore, can relieve the requirement on the MAS speed. However, a high magnetic field not only helps in increasing the sensitivity but also enhances the differences in CSA between various sites, thereby facilitating their measurement. Although the CSA-induced line broadening increases at high field, the application of the 2D MATPASS/CPMG technique solves that problem, as discussed above.

3. RESULTS AND DISCUSSION

An illustrative ^{77}Se 2D MATPASS/CPMG NMR spectrum is shown in Figure 2 for a sample of $Ge_{13}Se_{87}$ glass. The slices in the anisotropic dimension show a separation of the spinning sidebands (Figure 2d). A shear of the spectrum along F_2 that aligns all spinning sidebands with the isotropic peaks can then yield a spectrum correlating purely isotropic (horizontal) and anisotropic (vertical) dimensions, that is, a correlation between the isotropic chemical shift and CSA (Figure 2c). Once all slices along the anisotropic dimension are summed, an isotropic projection free of any CSA-induced broadening is obtained, which essentially represents a ^{77}Se MAS NMR spectrum collected at an infinite spinning rate (Figure 2b). A comparison of the ^{77}Se isotropic NMR spectrum of the $Ge_{13}Se_{87}$ glass with its regular ^{77}Se MAS NMR spectrum (Figure 2a) collected at a spinning rate of 10 kHz clearly shows a significant increase in resolution in the former spectrum due to the removal of the residual CSA-induced line broadening that is present even at a relatively fast sample spinning rate.

The ^{77}Se isotropic NMR spectra for all glass compositions are shown in Figure 3. These spectra are dominated by two peaks that display systematic compositional dependence in their position and intensity. The peak located at higher frequency (less shielded) in these ^{77}Se spectra can be unambiguously assigned to Se−**Se**−Se sites.[8,9,13,15,16] The intensity of this peak decreases and its position shifts to lower frequency with increasing Ge content from ∼850 ppm for Ge_5Se_{95} to ∼790 ppm for $Ge_{30}Se_{70}$. The clear separation of this high-frequency peak allows determination of the relative fraction of Se−**Se**−Se sites in these glasses with a significantly higher degree of accuracy compared to that of previous studies based on lower-resolution ^{77}Se NMR spectroscopy. The relative concentration of Se−**Se**−Se sites in these glasses, as obtained from the simulations of these ^{77}Se isotropic NMR spectra with Gaussian line shapes, is shown in Figure 4. The experimental variation is clearly not consistent with those expected from the two extreme models: neither the chain crossing model (Figure 4, red circles) based on the maximum avoidance of connectivity between the $GeSe_4$ tetrahedra, nor the clustering model (Figure

dx.doi.org/10.1021/jp311320t | J. Phys. Chem. B 2013, 117, 949−954

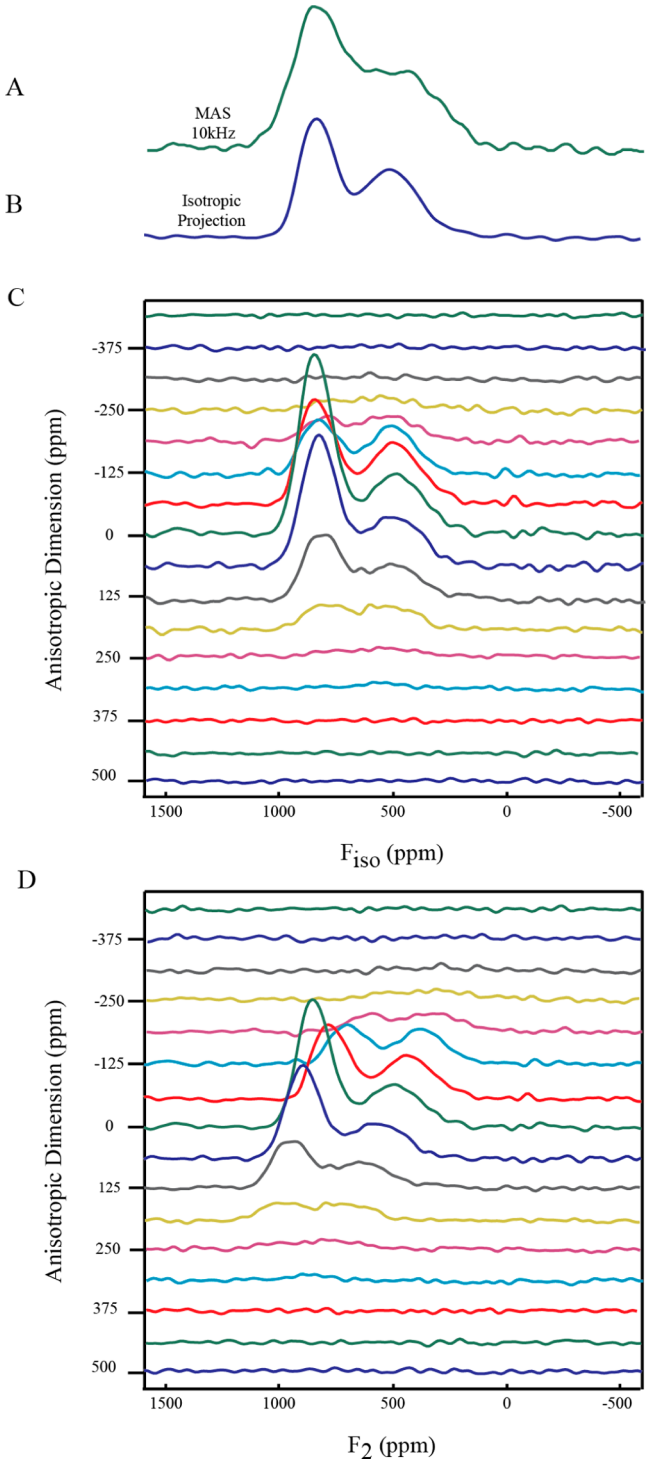

Figure 2. A comparison of the (A) 10 kHz MAS spectrum with the total isotropic projection of the (B) ^{77}Se 2D MATPASS/CPMG NMR spectrum of $Ge_{13}Se_{87}$ glass. The full ^{77}Se 2D MATPASS/CPMG NMR spectra are shown (C) after and (D) before F_2 shearing. The isotropic projection in (B) obtained by summation of spinning sidebands after F_2 shearing shows increased resolution over the MAS spectrum.

4, blue triangles) based on the complete segregation of the tetrahedral and chain elements in the network. Instead, the compositional dependence of the relative fraction of Se−**Se**−Se sites in these glasses appears to follow the trend expected from a stochastic random network model (Figure 4, green inverted triangles) where the $GeSe_4$ tetrahedra and the Se−Se chain

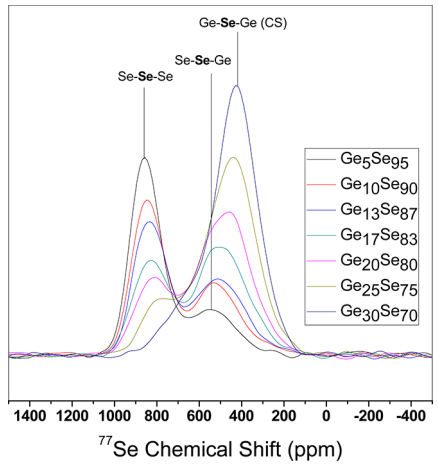

Figure 3. ^{77}Se isotropic NMR spectra of Ge_xSe_{100-x} glasses. Average δ_{iso} for the Se−**Se**−Se, Se−**Se**−Ge, and CS Ge−**Se**−Ge sites are shown with vertical lines.

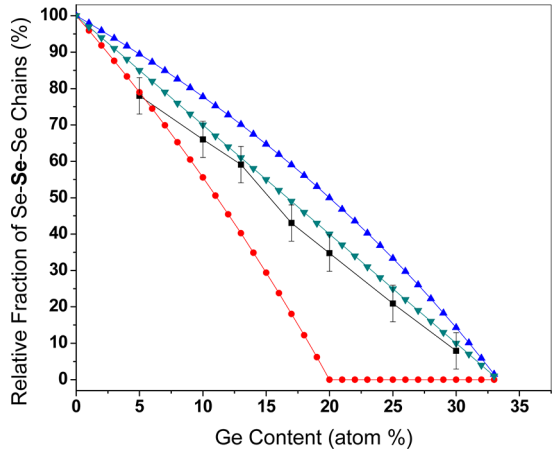

Figure 4. Compositional variation of the relative fraction of Se−**Se**−Se sites (black squares) is compared with the predictions for the chain crossing model (red circles), the clustering model (blue triangles), and the random network model (green inverted triangles).

elements are randomly connected to form the glass network. It may be noted here that previous high-temperature liquid ^{77}Se NMR studies also suggested random network structures for glasses in the P−Se and As−Se systems.[21,22] The nearly linear shift of the position of the isotropic peak corresponding to the Se−**Se**−Se sites in Figure 4 to lower frequencies with increasing Ge content (Figure 5) represents a systematic next-nearest-neighbor effect on the ^{77}Se NMR chemical shift. This effect is likely related to the increasing probability of a Ge atom being the next-nearest neighbor of a **Se** atom to form Ge−Se−**Se**−Se− structural moieties and terminate selenium chains as the Ge content of these glasses increases.

The lower-frequency peak in the ^{77}Se isotropic NMR spectrum of the Ge_5Se_{95} glass is centered at ~550 ppm (Figure 3). As mentioned above, earlier studies have assigned this ^{77}Se isotropic chemical shift to the Se−**Se**−Ge sites, although the ES Ge−**Se**−Ge sites are also expected to have similar δ_{iso} values.[13,16] Previous Raman spectroscopic studies have shown that the relative fraction of the ES Ge−**Se**−Ge environments is expected to be quite small in Ge_xSe_{100-x} glasses with low Ge concentrations similar to that of Ge_5Se_{95}. Therefore, the peak at ~550 ppm in the ^{77}Se isotropic NMR spectrum of the Ge_5Se_{95}

dx.doi.org/10.1021/jp311320t | J. Phys. Chem. B 2013, 117, 949−954

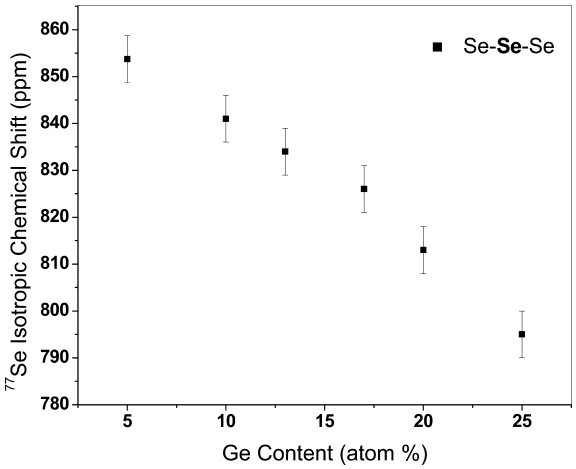

Figure 5. Compositional variation of the average δ_{iso} of Se−**Se**−Se sites.

glass can be assigned almost entirely to the Se−**Se**−Ge sites.[13,15,16] With increasing Ge content, the center of gravity of the low-frequency peak in these isotropic spectra shifts to lower chemical shift values (lower frequency). The low-frequency peak in the ^{77}Se isotropic NMR spectrum of the $Ge_{30}Se_{70}$ glass is dominated by a peak with $\delta_{iso} \approx 400$ ppm (Figure 3). This δ_{iso} is uniquely characteristic of the CS Ge−**Se**−Ge sites. A clear shoulder is observed on the high-frequency side of this peak near $\delta_{iso} \approx 550$ ppm in the ^{77}Se isotropic NMR spectrum of the $Ge_{20}Se_{80}$ glass (Figure 3). This result indicates that the composite nature of the low-frequency peak in these isotropic spectra is consistent with the coexistence of Se−**Se**−Ge and ES Ge−**Se**−Ge sites together with the CS Ge−**Se**−Ge sites in the glass structure. With increasing Ge concentration, the contribution to the peak at ~550 ppm from the ES Ge−**Se**−Ge sites becomes dominant over that from the Se−**Se**−Ge sites, as indicated by previous Raman spectroscopic results on these glasses.[13]

In addition to the isotropic chemical shift, the 2D MATPASS/CPMG NMR spectra provide complementary CSA information for each structural site. A vertical slice of the 2D MATPASS/CPMG NMR spectrum at any isotropic chemical shift yields the corresponding CSA powder pattern that can be simulated using the Herzfeld−Berger method to obtain the principal components of the chemical shift tensor. Additional structural information regarding the site symmetry and conformation for the various Se sites can be gained from the determination of the anisotropy and the asymmetry of the chemical shift tensor. Moreover, determination of CSA may also enable distinction between sites that may happen to have similar isotropic chemical shift but their site symmetries are different enough to lead to distinct CSA tensor parameters.

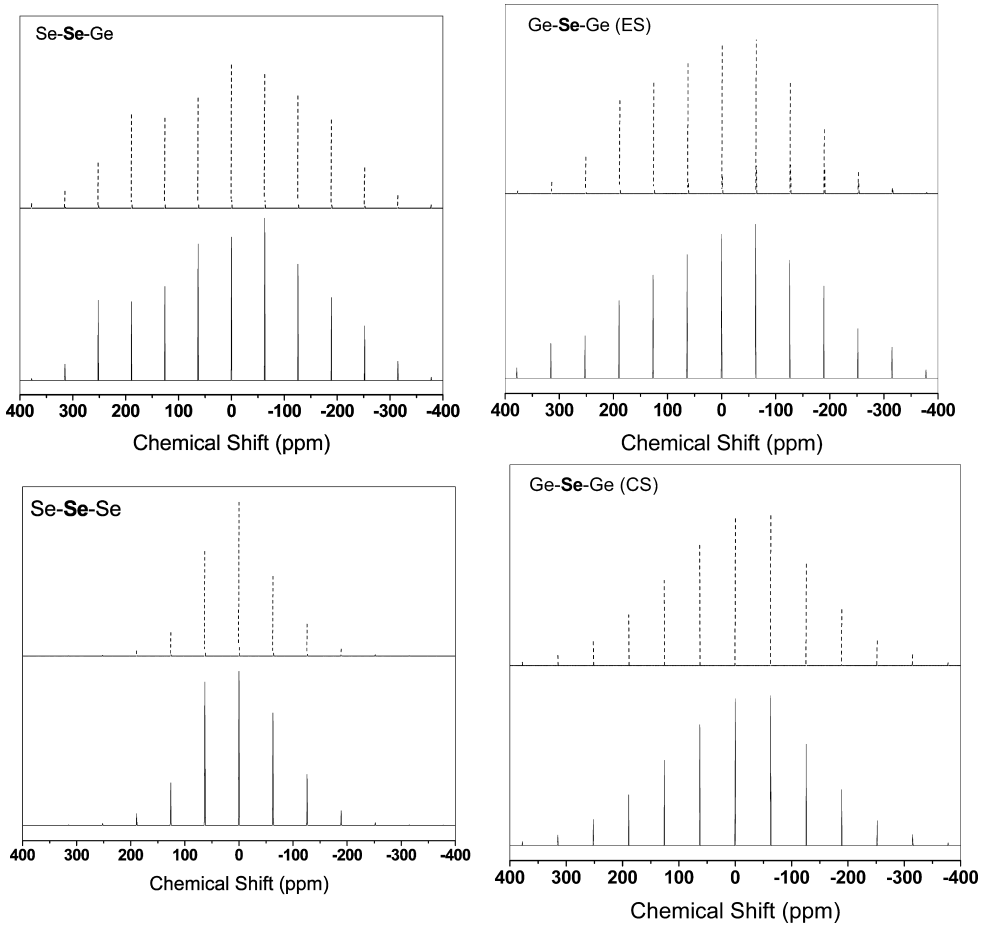

Figure 6. Comparison of the experimental (solid line) and simulated (dashed line) CSA sideband patterns for Se−**Se**−Se, Se−**Se**−Ge, ES Ge−**Se**−Ge, and CS Ge−**Se**−Ge sites. The Se−**Se**−Se and Se−**Se**−Ge slices were taken from the Ge_5Se_{95} compositions at δ_{iso} = 850 and 550 ppm, respectively. The ES and CS Ge−**Se**−Ge slices were taken at the $Ge_{30}Se_{70}$ composition at δ_{iso} = 410 and 600 ppm, respectively.

dx.doi.org/10.1021/jp311320t | J. Phys. Chem. B 2013, 117, 949−954

The CSA sideband patterns obtained from the ^{77}Se 2D MATPASS/CPMG NMR spectra were simulated in this study using the Herzfeld–Berger method with the software package DMFit[23] to obtain the principal components (δ_{11}, δ_{22}, and δ_{33}) of the chemical shift tensor parameters for the various Se sites in terms of the isotropic shift δ_{iso}, the asymmetry parameter η, and the reduced anisotropy δ_{aniso}. The CSA conventions used in this work are as follows:

$$|\delta_{33} - \delta_{iso}| \geq |\delta_{11} - \delta_{iso}| \geq |\delta_{22} - \delta_{iso}|$$

$$\eta = \frac{\delta_{11} - \delta_{22}}{\delta_{33} - \delta_{iso}}$$

$$\delta_{iso} = \frac{1}{3}(\delta_{11} + \delta_{22} + \delta_{33})$$

$$\delta_{aniso} = \delta_{33} - \delta_{iso}$$

The CSA sideband patterns for the Se–**Se**–Se, Se–**Se**–Ge, ES Ge–**Se**–Ge, and CS Ge–**Se**–Ge sites in these glasses are obtained as follows. On the basis of the peak assignments discussed above, the Se–**Se**–Se and Se–**Se**–Ge CSA projections were taken at the corresponding peak maxima of δ_{iso} = 850 and 550 ppm, respectively, in the ^{77}Se 2D MATPASS/CPMG NMR spectrum of the Ge_5Se_{95} glass. This glass composition and the peak maxima are chosen to minimize the contribution from any CS or ES Ge–**Se**–Ge sites in the CSA projections of the ^{77}Se NMR spectrum. On the other hand, the CSA sideband patterns for both the ES and CS Ge–**Se**–Ge sites were taken from the ^{77}Se 2D MATPASS/CPMG NMR spectrum of the $Ge_{30}Se_{70}$ composition as these Se environments are the most abundant at this composition and contributions from Se–**Se**–Se and Se–**Se**–Ge sites are minimized. The CSA projection for the CS Ge–**Se**–Ge site was taken at the corresponding peak maximum of δ_{iso} = 400 ppm, while the ES Ge–**Se**–Ge projection was taken at its characteristic δ_{iso} = 600 ppm. The CSA sideband patterns for these four Se sites and the corresponding Herzfeld–Berger simulations are shown in Figure 6. The CSA tensor parameters obtained from these simulations are summarized in Table 1. It

Table 1. ^{77}Se Chemical Shift Tensor Parameters for the Various Se Sites in Ge_xSe_{100-x} Glasses

sites	δ_{iso} (ppm)	δ_{aniso} (±10 ppm)	η (±0.1)
Se–**Se**–Se	850	−150	0.8
Se–**Se**–Ge	550	300	0.9
Ge–**Se**–Ge (CS)	400	250	0.9
Ge–**Se**–Ge (ES)	600	280	0.9

is instructive to note here that the magnitude of the anisotropy δ_{aniso} deviates increasingly from zero with increasing deviation from cubic site symmetry (i.e., perfect tetrahedral or octahedral symmetry). On the other hand, for the asymmetry parameter η ($0 \leq \eta \leq 1$), a departure from zero denotes deviation from axial symmetry. It is clear from Table 1 that the η values for the four Se sites are similar and vary between 0.8 and 0.9. These η values are consistent with those reported for the Se–**Se**–Se site in crystalline Se (η = 0.8) and for the Ge–**Se**–Ge sites in crystalline β-$GeSe_2$ (typically, $0.6 \leq \eta \leq 0.9$).[9,15] On the other hand, there is significant difference among these Se sites in their δ_{aniso} values (Table 1). Particularly interesting is the difference in δ_{aniso} between Se–**Se**–Se and other types of Se sites. While δ_{aniso} is relatively small and negative for the Se–**Se**–Se sites, it is positive and nearly twice as large for the other types of Se sites. A negative δ_{aniso} value was also reported[9] for the Se–**Se**–Se sites in crystalline Se, although the magnitude of δ_{aniso} for the crystalline phase is significantly larger (−250 ppm) compared to that in Ge_xSe_{100-x} glasses (−150 ppm, Table 1). The largest δ_{aniso} value of ∼300 ppm for the Se–**Se**–Ge site is consistent with the lack of symmetry for the central Se atom in its bonding environment, being bonded to dissimilar atoms on either side. On the other hand, the ES Ge–**Se**–Ge site is also characterized by a large δ_{aniso} value of ∼280 ppm that may result from the presence of a second Se atom, the edge-sharing pair, in close proximity to the Se site in question. This should be contrasted with the case of CS Ge–**Se**–Ge sites with relatively small δ_{aniso} (∼250 ppm), consistent with the higher site symmetry for the central Se atom in this environment compared to that for the ES site. A similar trend in the relative differences in δ_{aniso} for the CS and ES Ge–Se–Ge sites in crystalline β-$GeSe_2$ was also observed in a previous study where the typical magnitude of δ_{aniso} for the CS sites ranged between 350 and 470 ppm while that for the ES site was found to be ∼550 ppm.[15] However, all of these δ_{aniso} values for the CS and ES Ge–**Se**–Ge sites in crystalline β-$GeSe_2$ are significantly higher than their corresponding values (250–280 ppm) obtained for the Ge_xSe_{100-x} glasses in this study.

It is important to note that the δ_{aniso} for the Se–**Se**–Se sites decreases nearly linearly with increasing Ge content as well with the ^{77}Se δ_{iso} (Figure 7), signifying the effect of the presence of

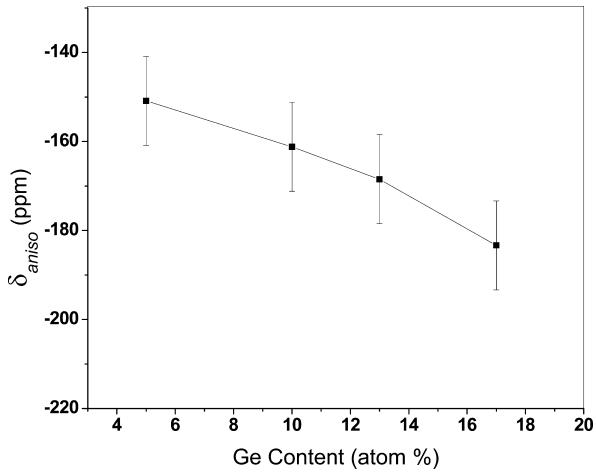

Figure 7. Compositional variation of the average δ_{aniso} value of Se–**Se**–Se sites.

Ge next-nearest neighbors, as discussed above to explain the composition dependence of ^{77}Se δ_{iso} of these sites. The presence of Ge atoms terminating the selenium chain fragments may alter the bond lengths and angles associated with the −Se–**Se**–Se− central moiety and thereby affect the local electronic shielding at the central **Se** nuclide. Therefore, the average ^{77}Se δ_{iso} and δ_{aniso} of the peak corresponding to the Se–**Se**–Se sites can be used as indicators of the chain length in these glasses. Future ab initio calculations of ^{77}Se δ_{iso} and δ_{aniso} for various selenium chain lengths terminated by Ge atoms will therefore be important in this regard to establish these NMR parameters as spectroscopic markers for the determination of average chain lengths. However, by the same token, the full width at half-maximum (fwhm) of the Se–**Se**–Se peak in the

dx.doi.org/10.1021/jp311320t | J. Phys. Chem. B 2013, 117, 949–954

^{77}Se isotropic NMR spectra of these glasses can be used as an indicator of the selenium chain length distribution. When plotted as a function of composition, the fwhm of the Se−**Se**−Se peak shows a maximum near 20 atom % Ge, indicating a corresponding maximum in the frozen-in configurational entropy of mixing (Figure 8). This result is consistent with

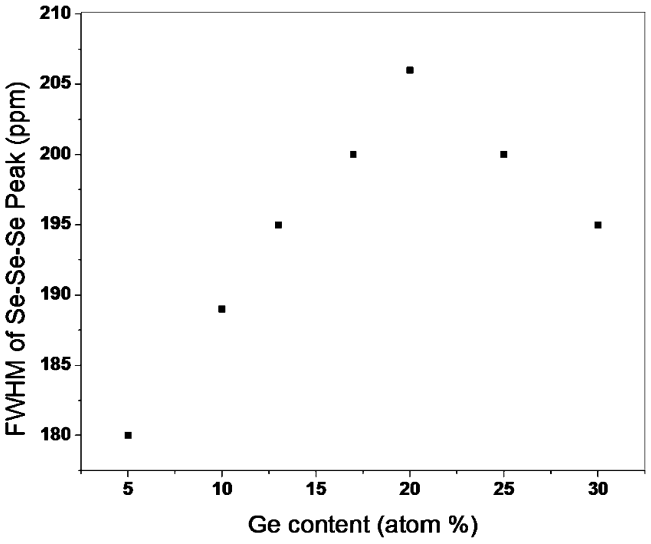

Figure 8. Compositional variation of the fwhm of the Se−**Se**−Se peak in the isotropic spectra in Figure 2.

the experimentally observed minimum in fragility and the highest glass-forming tendency or stability against crystallization near this glass composition along the Ge−Se binary join.[15,24,25]

4. SUMMARY

The ^{77}Se 2D MATPASS/CPMG NMR spectra of Ge_xSe_{100-x} glasses allow for the identification of Se−**Se**−Se, Ge−**Se**−Se, and CS and ES Ge−**Se**−Ge sites in the network, on the basis of their characteristic ^{77}Se δ_{iso} and CSA. The results clearly demonstrate the presence of connectivity between Ge−**Se**−Ge and Se−**Se**−Se sites via Ge−**Se**−Se linkages in the network. The compositional variation of the relative fraction of the Se−**Se**−Se sites is consistent with the model of a stochastic random network structure for these glasses that is formed by random interconnection between $GeSe_4$ tetrahedra and Se−Se chain fragments. The systematic dependence of δ_{iso} and CSA of the Se−**Se**−Se sites with Ge concentration indicates that the termination of Se chains by Ge next-nearest neighbors plays a significant role in influencing the local electronic environment around the central Se atom. These results can potentially be combined with ab initio calculations in the future to determine the average Se chain lengths in selenide glasses.

AUTHOR INFORMATION

Notes

The authors declare no competing financial interest.

ACKNOWLEDGMENTS

This work was supported by the National Science Foundation Grant DMR GOALI-1104869. The National High Magnetic Field Laboratory is supported through the National Science Foundation Cooperative Agreement (DMR-0084173) and by the State of Florida.

REFERENCES

(1) Zakery, A.; Elliott, S. R. *J. Non-Cryst. Solids* **2003**, *330*, 1.
(2) Bureau, B.; Zhang, X. H.; Smektala, F.; Adam, J. L.; Troles, J.; Ma, H. L.; Boussard-Pledel, C.; Lucas, J.; Lucas, P.; Le Coq, D.; Riley, M. R.; Simmons, J. H. *J. Non-Cryst. Solids* **2004**, *345*, 276.
(3) Sanghera, J. S.; Aggarwal, I. D. *J. Non-Cryst. Solids* **1999**, *256−257*, 6.
(4) Bychkov, E.; Benmore, C. J.; Price, D. L. *Phys. Rev. B* **2005**, *72*, 172107.
(5) Petri, I.; Salmon, P. S.; Fischer, H. E. *Phys. Rev. Lett.* **2000**, *84*, 2413.
(6) Salmon, P. S. *J. Non-Cryst. Solids* **2007**, *353*, 2959.
(7) Salmon, P. S.; Petri, I. *J. Phys.: Condens. Matter* **2003**, *15*, S1509.
(8) Bureau, B.; Troles, J.; Le Floch, M.; Guenot, P.; Smektala, F.; Lucas, J. *J. Non-Cryst. Solids* **2003**, *319*, 145.
(9) Bureau, B.; Troles, J.; Le Floch, M.; Smektala, F.; Lucas, J. *J. Non-Cryst. Solids* **2003**, *326&327*, 58.
(10) Lucas, P.; King, E. A.; Gulbiten, O.; Yarger, J. L.; Soignard, E.; Bureau, B. *Phys. Rev. B* **2009**, *80*, 214114.
(11) Sugai, S. *Phys. Rev. B* **1987**, *35*, 1345.
(12) Edwards, T. G.; Sen, S. *J. Phys. Chem. B* **2011**, *115*, 4307.
(13) Edwards, T. G.; Sen, S.; Gjersing, E. L. *J. Non-Cryst. Solids* **2012**, *358*, 609.
(14) Gjersing, E. L.; Sen, S.; Youngman, R. E. *Phys. Rev. B* **2010**, *82*, 014203.
(15) Gjersing, E. L.; Sen, S.; Aitken, B. G. *J. Phys. Chem. C* **2010**, *114*, 8601.
(16) Kibalchenko, M.; Yates, J. R.; Massobrio, C.; Pasquarello, A. *Phys. Rev. B* **2010**, *82*, 020202.
(17) Kibalchenko, M.; Yates, J. R.; Massobrio, C.; Pasquarello, A. *J. Phys. Chem. C* **2011**, *115*, 7755.
(18) Hung, I.; Edwards, T.; Sen, S.; Gan, Z. *J. Magn. Reson.* **2012**, *221*, 103.
(19) Hung, I.; Gan, Z. H. *J. Magn. Reson.* **2010**, *204*, 150.
(20) States, D. J.; Haberkorn, R. A.; Ruben, D. J. *J. Magn. Reson.* **1982**, *48*, 286.
(21) Rosenhahn, C.; Hayes, S. E.; Rosenhahn, B.; Eckert, H. *J. Non-Cryst. Solids* **2001**, *284*, 1.
(22) Maxwell, R.; Lathrop, D.; Eckert, H. *J. Non-Cryst. Solids* **1995**, *180*, 244.
(23) Massiot, D.; Fayon, F.; Capron, M.; King, I.; Le Calvé, S.; Alonso, B.; Durand, J. O.; Bujoli, B.; Gan, Z.; Hoatson, G. *Magn. Reson. Chem.* **2002**, *40*, 70.
(24) Azoulay, R.; Thibierge, H.; Brenac, A. *J. Non-Cryst. Solids* **1975**, *18*, 33.
(25) Phillips, J. C. *J. Non-Cryst. Solids* **1979**, *34*, 153.